Geomech. Geophys. Geo-energ. Geo-resour. (2023) 9:64
https://doi.org/10.1007/s40948-023-00613-4

ORIGINAL ARTICLE

Check for updates

# Analysis and verification of stress and plastic zone in surrounding rocks of hydraulic flushing borehole based on strain-softening

**Junqi Cui · Yunbing Hou · Shengrong Xie · Dongdong Chen · Xiangxiang Yan · Yuxin Ren**

Received: 26 August 2022 / Accepted: 9 May 2023


**Abstract** This study aimed to solve the problem ignored by previous research on hydraulic flushing gas extraction technology regarding the strain-softening of surrounding rock. Firstly, through the analysis of experimental data, previous studies have proved that the essence of strain-softening is that the internal friction angle remains unchanged while the cohesion decreases. According to the variation law of cohesion of surrounding rocks in a borehole, we theoretically analyzed the stress distribution of the surrounding rock considering strain-softening and determined the theoretical formula of the plastic zone radius. Subsequently, we established a numerical calculation model considering strain-softening using the COMSOL numerical simulation software. We simulated the influence of residual cohesion on the stress and plastic zone of surrounding rocks of the borehole. We found that with the decrease in residual cohesion, the peak stress transferred to the deep and the plastic zone radius gradually increased. The simulation results were compared with the theoretical values, and the errors were found to be within 10%, which verifies the model's accuracy. Subsequently, we studied the influence law of strain-softening on the stress and plastic zone of surrounding rocks of boreholes with different radii. We found that the larger the borehole radius, the greater the influence of strain-softening. The field measurement results show that the stress reduction zone of a hydraulic flushing borehole is about 10 times the borehole radius. The stress reduction zone calculated without considering strain-softening is 1.305 times the borehole radius, and that calculated while considering strain-softening is 6.663 times the borehole radius. Thus, we proved that strain-softening is an essential factor affecting the stress distribution of surrounding rocks of the borehole. When studying the gas extraction through a hydraulic flushing borehole, it is necessary to consider the strain-softening of surrounding rocks.

**Article highlights**

- The stress distribution of borehole surrounding rock considering strain-softening is analyzed theoretically.
- The influence of residual cohesion on the stress and plastic zone of the borehole surrounding rock is studied by numerical simulation.
- Field examples prove that there is strain-softening in the engineering.

J. Cui · Y. Hou · S. Xie (✉) · D. Chen · X. Yan · Y. Ren
School of Energy and Mining Engineering, China University of Mining and Technology, Beijing, Beijing 100083, China
e-mail: xsrxcq@163.com

Published online: 22 May 2023

**Keywords** Hydraulic flushing borehole · Strain-softening · Residual cohesion · Stress evolution of surrounding rock · Plastic zone radius · Field measurement

## 1 Introduction

Pre-drainage of the coal seam gas through an underground borehole is the primary means of coal mine gas control (Lin and Zhang 1996; Zhang 2001). However, in China, coal seams generally have soft coal and low permeability, which results in unsatisfactory gas control by ordinary boreholes (Ge et al. 2014; Wang et al. 2015; Wei et al. 2016; Cao et al. 2018). Introducing a high-pressure water jet has improved the hydraulic flushing technology in coal mines because of its fast outburst elimination speed and high extraction efficiency. The construction principle of hydraulic flushing technology is shown in Fig. 1. This technology uses a high-pressure water jet to break coal and can expand the diameter of ordinary drilling several times or even more.

With the application of hydraulic flushing technology, experts and scholars have conducted substantial research on its antireflection effect and achieved some reasonable results (Wang et al. 2012; Li et al. 2015; Tao et al. 2018). Liu et al. (2005) and Kong et al. (2005) successfully applied hydraulic flushing technology to achieve coal seam outburst effectively and clarify its process flow. Liu et al. (2009) analyzed the antireflection effect of hydraulic flushing by investigating the parameters such as the amount of coal flushing in a single borehole, gas volume fraction before and after flushing, and volume of single borehole gas extraction. Wang et al. (2011) introduced the process of a hydraulic flushing test using cross-measure boreholes and studied the gas extraction radius of hydraulic flushing. Wang et al. (2013) investigated the pressure relief range of hydraulic flushing in the field using the gas pressure and gas content methods. Using numerical simulation software, they analyzed the variation law of coal stress and permeability around a hydraulic flushing borehole. Hao et al. (2014) established a seepage stress coupling model considering the dynamic change of permeability and adsorption characteristics, studied the flushing radius of boreholes with different coal flushing volumes, and optimized the hole layout parameters of hydraulic flushing. Gao et al. (2015) discussed the influence of increasing the borehole diameter through hydraulic flushing on the coal seam permeability. Field application shows that when the borehole diameter is 1.0 m, the effective influence radius can reach 4 m. Kong et al. (2016) studied the coupling effect of the borehole radius, initial gas pressure, and other factors on the effective influence radius using the response surface method, and found a good corresponding relationship between the gas pressure distribution and stress distribution. Zhang and Wang (2017) studied the gas extraction effect after applying hydraulic flushing technology

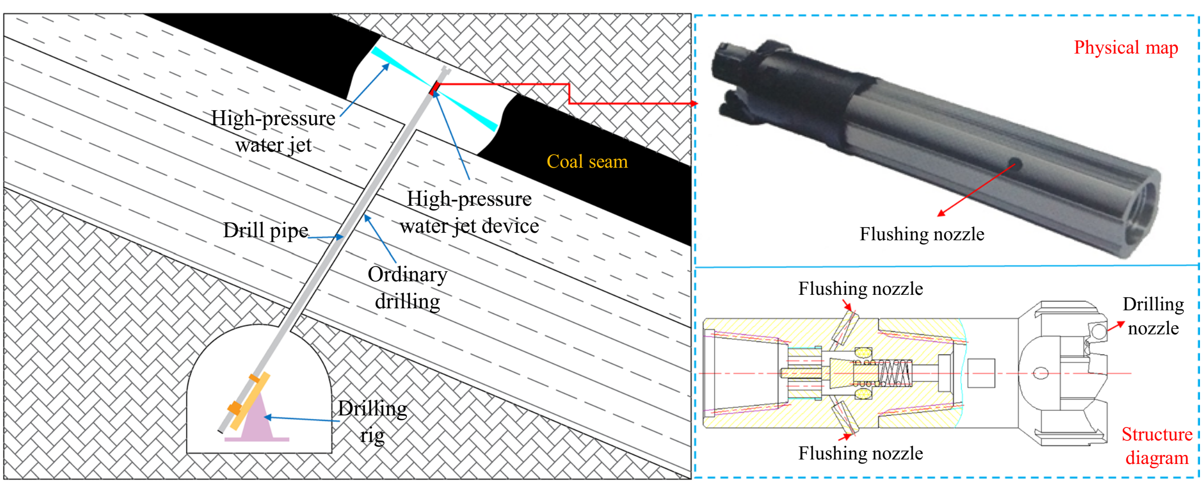


**Fig. 1** Schematic diagram of hydraulic punching construction

based on the fluid–structure coupling theory of coal seam gas flow. They found that the effective influence radius of multiple boreholes is significantly greater than that of a single borehole. Shen et al. (2018) used the electromagnetic radiation method to evaluate the effect of cross-measure boreholes on hydraulic flushing. Zhang et al. (2019) combined the gas diffusion, gas flow, and permeability model by considering the effects of stress change and plastic failure, established a new fully coupled gas extraction model, and studied the mechanism of hydraulic flushing by numerical simulation to strengthen gas extraction. Chen et al. (2020) built a multi-physical coupling model based on the strain-softening constitution and Mohr–Coulomb failure criterion related to the gas pressure and second principal stress, and studied the failure range and permeability evolution after hydraulic flushing. Thereafter, Cao et al. (2021) established a fluid–structure coupling model of coal-containing gas with low permeability, and simulated and analyzed the temporal and spatial evolution law of the coal gas pressure and borehole diameter around hydraulic flushing boreholes in short-range outburst coal seams by using the COMSOL Multiphysics numerical simulation software. Zhang et al. (2022) established a multi-physical field coupling model, and analyzed the mechanism of hydraulic flushing to strengthen gas extraction using the numerical simulation method of FLAC3D and COMSOL.

It can be seen from the above that, in summary, experts and scholars have gradually deepened their research on hydraulic flushing technology, and theoretical research has also changed from single gas research to fluid–structure coupling. However, the study on the solid part of the surrounding rock of the hydraulic flushing borehole is mainly based on the Mohr–Coulomb model. Their research shows that in the excavation process, owing to the continuous expansion of microcracks in the rock, the strength parameters of surrounding rocks decrease significantly in the nonlinear stage, namely, the so-called surrounding rock softening phenomenon (Zhou et al. 2009; Leandro et al. 2012; Cao et al. 2013). Furthermore, the strain softening model is applied to engineering practice. For example, Gao et al. (2020) derived the calculation of the stress field of surrounding rocks of a tunnel and the displacement of the plastic zone by combining the strain-softening model and the non-associative flow law. He et al. (2021) proposed a method for analyzing the strain-softened slope progressive damage mode and stability reliability under multifield coupling conditions by considering the effects of groundwater level fluctuations and seismic forces. Following this, Liang et al. (2022) established a method to determine the optimal support timing for tunnels by reasonably considering the strain-softening characteristics after the rock peak.

The formation of a hydraulic flushing borehole is also a typical excavation problem. When the Mohr–Coulomb model is used to study it, the results will have errors due to the neglect of reducing the post-peak strength of coal and rock. Thus, it is necessary to consider the strain-softening of coal when studying this process. Based on previous experimental research, this paper discusses the essence of strain-softening of coal and rock, theoretically analyzes the stress distribution around the hydraulic flushing borehole by considering strain-softening, applies the strain-softening model to the COMSOL numerical simulation software, and studies the influence of strain-softening of coal and rock on the stress and plastic zone distributions of a hydraulic flushing borehole.

## 2 The essence of strain-softening of coal and rock

The original data in the four published papers are selected for analysis to study the essence of strain-softening of coal and rock. The original stress–strain curve is shown in Fig. 2 (Zuo et al. 2016; Wang et al. 2021; Zhang and Zhao 2014; Su and Fu 2014). This figure shows that with the increase of coal and rock strain, the strength decreases rapidly after reaching the peak stress $\sigma_{\mathrm{p}}$, and the strength of coal and rock tends to be flat, defined as the residual strength $\sigma_r$.

According to the Mohr–Coulomb theory, the corresponding strength criterion of coal and rock at peak strength and residual strength can be expressed by Eqs. (1) and (2) (Jing et al. 2018):

$$\sigma_1 = \frac{1+\sin\varphi_p}{1-\sin\varphi_p}\sigma_3 + \frac{2c_p\cos\varphi_p}{1-\sin\varphi_p} \tag{1}$$

$$\sigma_1 = \frac{1+\sin\varphi_r}{1-\sin\varphi_r}\sigma_3 + \frac{2c_r\cos\varphi_r}{1-\sin\varphi_r} \tag{2}$$

where $\sigma_3$ is confining pressure, MPa; $\varphi_p$ is the internal friction angle corresponding to the peak strength of coal and rock, °; $c_p$ is the cohesion corresponding

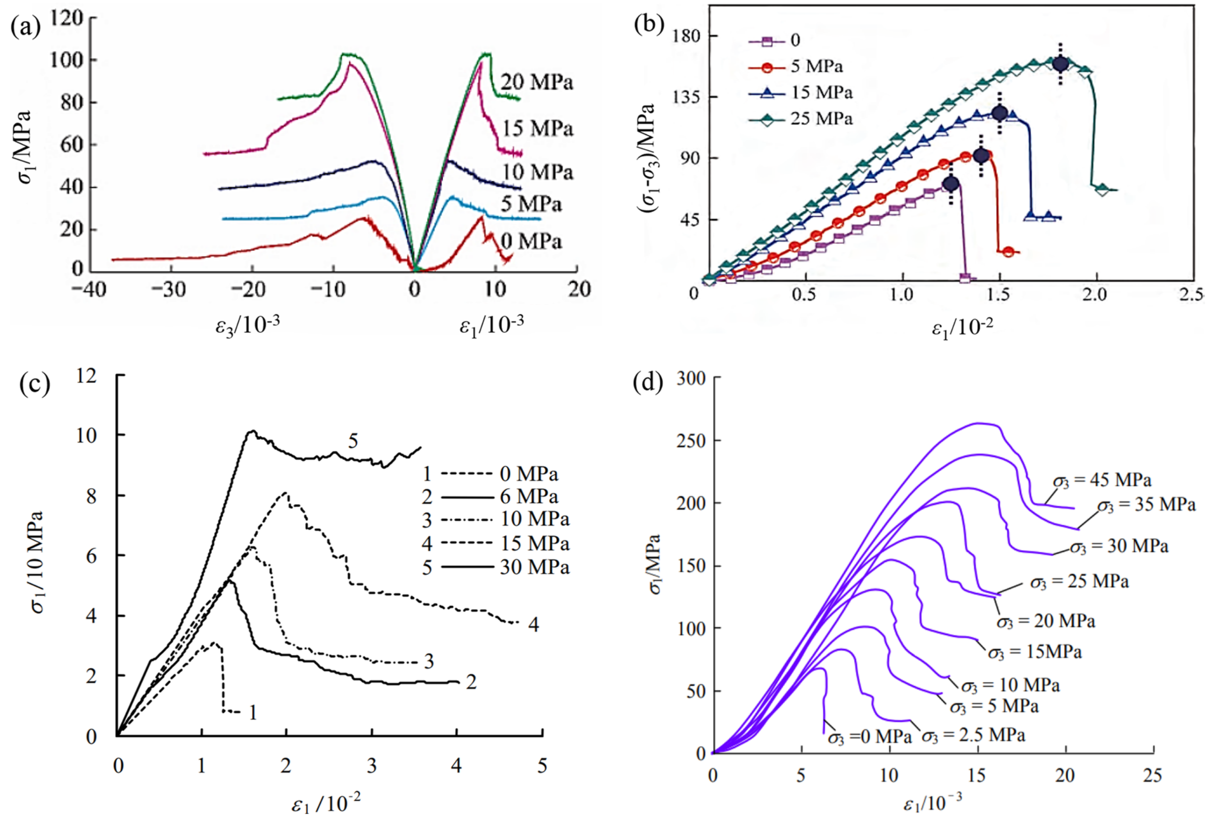


**Fig. 2** Original stress–strain curve: **a** Zuo et al. (2016); **b** Wang et al. (2021); **c** Zhang and Zhao (2014); and **d** Su and Fu (2014)

to the peak strength of coal and rock, MPa; $\varphi_r$ is the internal friction angle corresponding to the residual strength of coal and rock, °; and $c_r$ is the cohesion corresponding to the residual strength of coal and rock, MPa.

As can be seen from the formula, in the $\sigma_1$-$\sigma_3$ coordinate, $\sigma_1$ is directly proportional to $\sigma_3$. The internal friction angle corresponding to the peak and residual strength values can be determined according to the slope, and the cohesion corresponding to the peak and residual strength values can be determined based on the intercept and internal friction angle. The peak and residual strength values of coal and rock under different confining pressures obtained from four published literature are presented in Table 1. According to the confining pressure, peak strength, and residual strength data presented in Table 1, the curve shown in Fig. 3 can be obtained.

Figure 3 shows that the peak strength and residual strength of coal and rock fit well with the confining pressure $\sigma_3$. According to the appropriate formula and the strength criterion corresponding to the peak strength and residual strength of coal and rock, we can calculate the peak internal friction angle $\varphi_p$ and residual internal friction angle $\varphi_r$, peak cohesion $c_p$, and residual cohesion $c_r$ of coal and rock in the literature. The results are presented in Tables 2 and 3.

As presented in Table 2, the residual internal friction angle $\varphi_r$ of coal and rock changed slightly compared with the peak internal friction angle $\varphi_p$. The change in the maximum internal friction angle is 6.3310°, while the minimum internal friction angle changed by 0.2070°. It should be noted that those in the residual internal friction angle vary compared with the peak internal friction angle, showing both increasing and decreasing trends; the rate of change of the average internal friction angle is only 1.9399%. As presented in Table 3, the residual cohesion $c_r$ of coal and rock changes significantly compared with the peak cohesion $c_p$. The minimum and maximum rates of change of cohesion are −65.5716 and −99.3381%, respectively; the

Table 1 Peak strength and residual strength of coal and rock under different confining pressures

| Literature | Confining pressure $\sigma_3$/MPa | Peak strength $\sigma_p$/MPa | Residual strength $\sigma_r$/MPa |
|---|---|---|---|
| Zuo et al. (2016) | 0 | 25.44 | 3.42 |
| | 5 | 35.38 | 25.07 |
| | 10 | 52.38 | 40.82 |
| | 15 | 97.95 | 58.95 |
| | 20 | 102.8 | 82.91 |
| Wang et al. (2021) | 0 | 74.50 | 1.74 |
| | 5 | 97.51 | 25.81 |
| | 15 | 137.01 | 60.52 |
| | 25 | 184.85 | 90.49 |
| Zhang and Zhao (2014) | 0 | 30.90 | 7.80 |
| | 6 | 51.60 | 17.70 |
| | 10 | 62.50 | 23.10 |
| | 15 | 80.70 | 38.50 |
| | 30 | 100.90 | 93.70 |
| Su and Fu (2014) | 0 | 68.00 | 0.00 |
| | 2.5 | 83.10 | 28.70 |
| | 5 | 100.90 | 54.90 |
| | 10 | 130.30 | 79.90 |
| | 15 | 153.40 | 99.20 |
| | 20 | 172.30 | 136.40 |
| | 25 | 200.30 | 153.80 |
| | 30 | 212.30 | 180.30 |
| | 35 | 238.30 | 180.30 |
| | 45 | 263.70 | 198.40 |

average rate of change of cohesion is −84.2219%. Additionally, the rates of change of cohesion are negative, namely, the residual cohesion decreases compared with the peak cohesion. Based on the above analysis, we inferred that the essence of the strain-softening of coal and rock is that the internal friction angle remains unchanged, and the cohesion decreases.

The stress–strain curve of coal and rock can be simplified by the "3-line representation," as shown in Fig. 4. It is divided into the elastic, plastic, and residual stages. The cohesion in the elastic stage is peak cohesion $c_p$, and that in the residual stage is residual cohesion $c_r$. According to the previous research results, the change of coal and rock cohesion corresponding to the stress–strain curve can be expressed by the following equation (Jaiswal and Shrivastva 2009):

$$c = \begin{cases} c_p, \gamma^p = 0 \\ c_s, 0 < \gamma^p < \gamma^{p^*} \\ c_r, \gamma^p \geq \gamma^{p^*} \end{cases} \tag{3}$$

where $c_s$ is the cohesion of coal and rock in the plastic stage, MPa; $\gamma^p$ is the equivalent plastic shear strain; and $\gamma^{p^*}$ is the equivalent plastic shear strain at the beginning of the residual stage, 0.01.

The cohesion in the plastic stage can be expressed as follows:

$$c_s = c_p - \frac{c_p - c_r}{\gamma^{p^*}}\gamma^p \tag{4}$$

The equivalent plastic shear strain can be expressed as the plastic principal strain as follows (Alonso et al. 2003; Joshua et al. 2019):

$$\gamma^p = \sqrt{\frac{2}{3}\left(\varepsilon_1^p\varepsilon_1^p + \varepsilon_2^p\varepsilon_2^p + \varepsilon_3^p\varepsilon_3^p\right)} \tag{5}$$

where $\varepsilon_1^p$, $\varepsilon_2^p$, and $\varepsilon_3^p$ are the first, second, and third principal plastic strains, respectively.

## 3 Stress distribution of borehole surrounding rock considering strain-softening

After borehole construction, owing to the redistribution of stress, the coal around the borehole can be divided into crushing, plastic, and elastic zones. The cohesion of each zone is shown in Fig. 5. For axisymmetric problems, the stress around the borehole meets the equilibrium differential equation, and the strength criterion is satisfied in the crushing and plastic zones. The equilibrium differential equation and the strength criterion in the crushing and plastic zones can be expressed by the following equations, respectively (Pan et al. 2018; Wang and Qian 2018):

$$\frac{d\sigma_r}{dr} + \frac{\sigma_r - \sigma_\theta}{r} = 0 \tag{6}$$

$$\sigma_\theta^r = \frac{1 + \sin\varphi}{1 - \sin\varphi}\sigma_r^r + \frac{2c_r\cos\varphi}{1 - \sin\varphi} \tag{7}$$

$$\sigma_\theta^s = \frac{1 + \sin\varphi}{1 - \sin\varphi}\sigma_r^s + \frac{2c_s\cos\varphi}{1 - \sin\varphi} \tag{8}$$

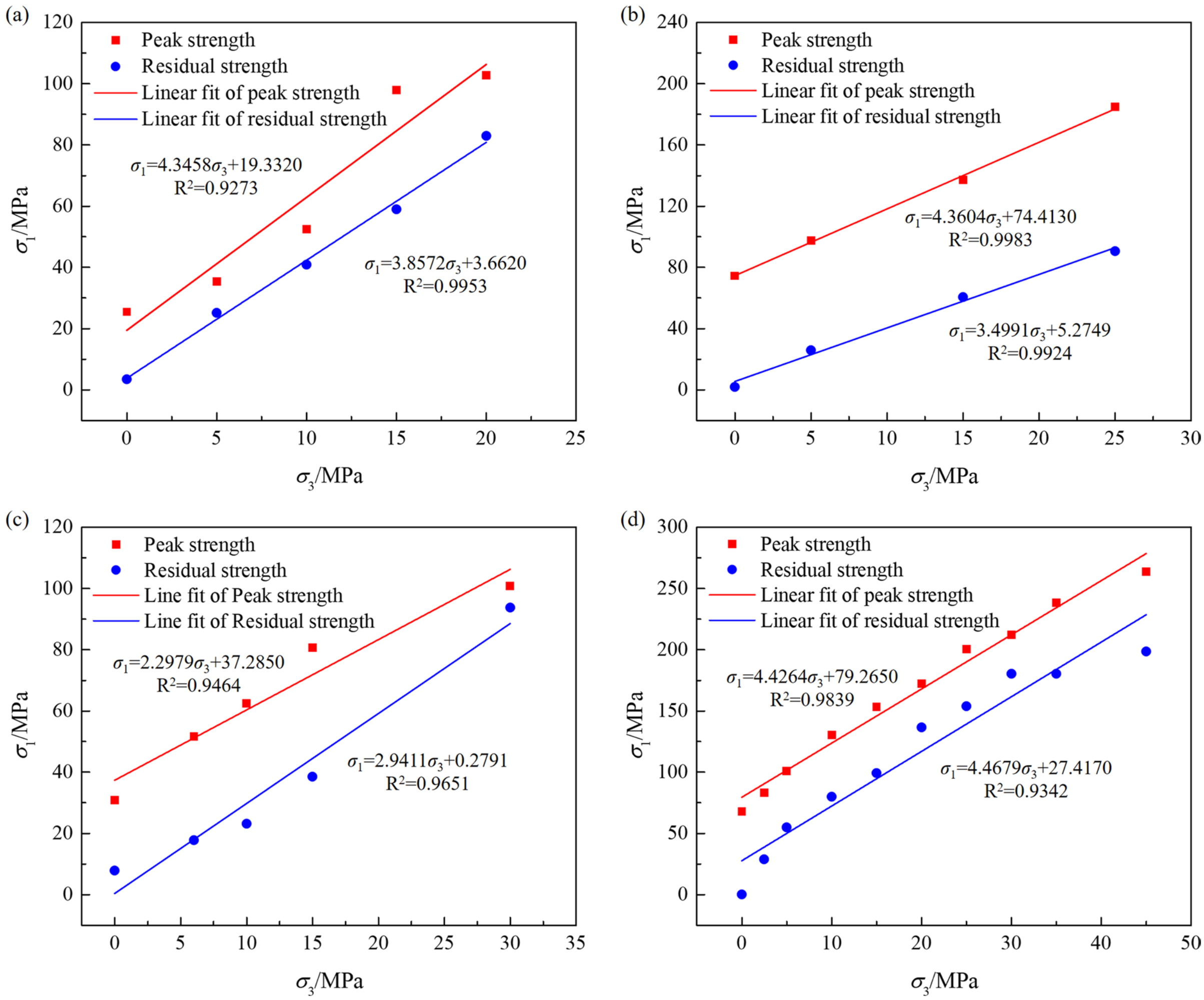


**Fig. 3** Fitting curve of the peak strength and residual strength from: **a** Zuo et al. (2016); **b** Wang et al. (2021); **c** Zhang and Zhao (2014); and **d** Su and Fu (2014)

**Table 2** Calculation results of the peak internal friction angle $\varphi_p$ and residual internal friction angle $\varphi_r$

| Literature | Peak internal friction angle $\varphi_p$/° | Residual internal friction angle $\varphi_r$/° | Variation of internal friction/° | Change rate of internal friction angle/% |
|---|---|---|---|---|
| Zuo et al. (2016) | 38.7464 | 36.0322 | −2.7142 | −7.0050 |
| Wang et al. (2021) | 38.8213 | 33.7429 | −5.0784 | −13.0815 |
| Zhang and Zhao (2014) | 23.1758 | 29.5068 | 6.3310 | 27.3173 |
| Su and Fu (2014) | 39.1558 | 39.3628 | 0.2070 | 0.5287 |
| Average | 34.9748 | 34.6612 | −0.3136 | 1.9399 |

where $\sigma_r$ is the radial stress, MPa; $\sigma_\theta$ is the tangential stress, MPa; $r$ is the distance from the borehole center, m; $\varphi$ is the internal friction angle, °; $\sigma_r^{r}$ is the radial stress in the crushing zone, MPa; $\sigma_\theta^{r}$ is the tangential stress in the crushing zone, MPa; $\sigma_r^{s}$ is the

**Table 3** Calculation results of the peak cohesion $c_p$ and residual cohesion $c_r$

| Literature | Peak cohesion $c_p$/MPa | Residual cohesion $c_r$/MPa | Variation of cohesion/MPa | Change rate of cohesion /% |
|---|---|---|---|---|
| Zuo et al. (2016) | 4.6366 | 0.9324 | −3.7042 | −79.8904 |
| Wang et al. (2021) | 17.8177 | 1.4098 | −16.4079 | −92.0876 |
| Zhang and Zhao (2014) | 12.2972 | 0.0814 | −12.2158 | −99.3381 |
| Su and Fu (2014) | 18.8388 | 6.4859 | −12.3529 | −65.5716 |
| Average | 13.3976 | 2.2274 | −11.1702 | −84.2219 |

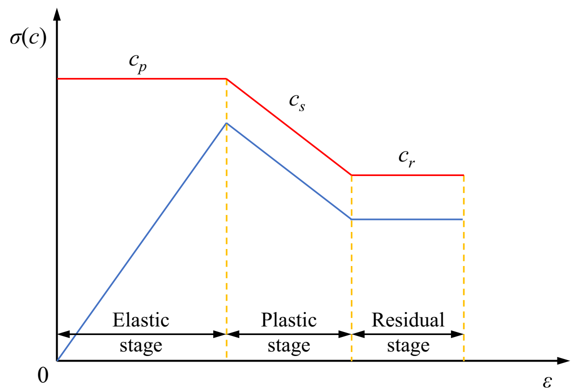


**Fig. 4** Simplified diagram of the stress–strain curve and corresponding cohesion

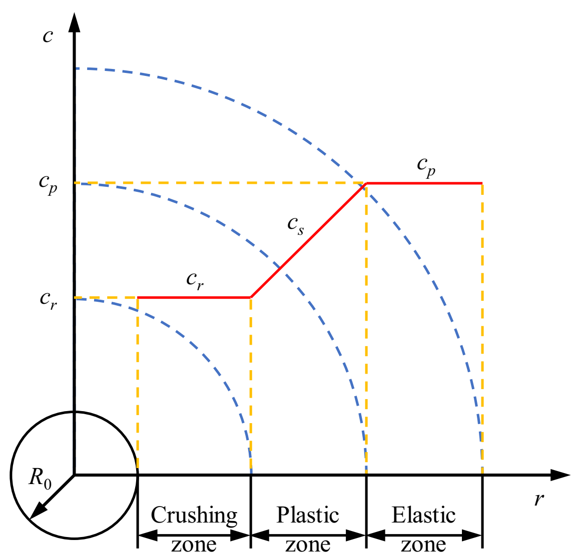


**Fig. 5** Coal zoning around the borehole and corresponding cohesion

radial stress in the plastic zone, MPa; and $\sigma_\theta^s$ is the tangential stress in the plastic zone, MPa.

## 3.1 Stress distribution in the crushing zone

The stress of the surrounding rocks of the borehole in the crushing zone followed the differential equation of stress balance and the strength criterion equation of the crushing zone simultaneously. Substituting Eq. (7) into Eq. (6), we obtained:

$$\frac{d\sigma_r^r}{dr}+\frac{\left(1-\frac{1+\sin\varphi}{1-\sin\varphi}\right)\sigma_r^r-\frac{2c_r\cos\varphi}{1-\sin\varphi}}{r}=0 \tag{9}$$

The calculation result is as follows:

$$\sigma_r^r=\frac{(1-\sin\varphi)C_1\cdot r^{\frac{2\sin\varphi}{1-\sin\varphi}}-2c_r\cos\varphi}{2\sin\varphi} \tag{10}$$

where $C_1$ is a constant.

The following boundary conditions exist in the crushing zone: when $r=R_0$, $\sigma_r=0$. Substituting this into Eq. (10), we obtained:

$$C_1=\frac{2c_r\cos\varphi}{1-\sin\varphi}R_0^{\frac{2\sin\varphi}{\sin\varphi-1}} \tag{11}$$

where $R_0$ is the borehole radius, m.

The radial stress distribution formula in the crushing zone can be obtained as follows by substituting Eq. (11) into Eq. (10):

$$\sigma_r^r=\frac{c_r\cos\varphi}{\sin\varphi}\left(R_0^{\frac{2\sin\varphi}{\sin\varphi-1}}r^{\frac{2\sin\varphi}{1-\sin\varphi}}-1\right) \tag{12}$$

The radial stress distribution formula in the crushing zone can be obtained as follows by substituting Eq. (11) into Eq. (10):

$$\sigma_\theta^r=\frac{c_r\cos\varphi}{\sin\varphi}\left(\frac{1+\sin\varphi}{1-\sin\varphi}R_0^{\frac{2\sin\varphi}{\sin\varphi-1}}r^{\frac{2\sin\varphi}{1-\sin\varphi}}-1\right) \tag{13}$$

### 3.2 Stress distribution in the plastic zone

In the plastic zone, the stress of the surrounding rocks of the borehole followed the differential equation of stress balance (6) and the strength criterion equation of the plastic zone (8), which can be obtained by substituting Eq. (8) into Eq. (6):

$$\frac{d\sigma_r^s}{dr} + \frac{\left(1 - \frac{1+\sin\varphi}{1-\sin\varphi}\right)\sigma_r^s - \frac{2c_s\cos\varphi}{1-\sin\varphi}}{r} = 0 \tag{14}$$

The calculation result is as follows:

$$\sigma_r^s = \frac{(1-\sin\varphi)C_2 \cdot r^{\frac{2\sin\varphi}{1-\sin\varphi}} - 2c_s\cos\varphi}{2\sin\varphi} \tag{15}$$

where $C_2$ is a constant.

The following boundary conditions exist in the plastic zone: when $r=R_r$, $\sigma_r{}^r=\sigma_r{}^s$, and $c_r=c_s$. Substituting this into Eq. (15), we obtained the following:

$$C_2 = \frac{2c_r\cos\varphi}{1-\sin\varphi} R_0^{\frac{2\sin\varphi}{\sin\varphi-1}} \tag{16}$$

The radial stress distribution formula in the plastic zone can be obtained as follows by substituting Eq. (16) into Eq. (15):

$$\sigma_r^s = \frac{\cos\varphi}{\sin\varphi}\left(c_r R_0^{\frac{2\sin\varphi}{\sin\varphi-1}} r^{\frac{2\sin\varphi}{1-\sin\varphi}} - c_s\right) \tag{17}$$

The tangential stress distribution formula in the plastic zone can be obtained as follows by substituting Eq. (17) into Eq. (6):

$$\sigma_\theta^s = \frac{\cos\varphi}{\sin\varphi}\left(c_r \frac{1+\sin\varphi}{1-\sin\varphi} r^{\frac{2\sin\varphi}{1-\sin\varphi}} R_0^{\frac{2\sin\varphi}{\sin\varphi-1}} - c_s\right) \tag{18}$$

At the junction of the plastic and elastic zones, when $r=R_s$, the stress showed the following relationship:

$$\sigma_r^s + \sigma_\theta^s = 2\sigma_0 \tag{19}$$

where $\sigma_0$ is the initial in-situ stress, MPa.

The radius of the plastic zone can be obtained as follows by using Eqs. (17) and (18):

$$R_s = R_0\left[\frac{1-\sin\varphi}{c_r}\left(\frac{\sigma_0\sin\varphi}{\cos\varphi} - c_s\right)\right]^{\frac{1-\sin\varphi}{2\sin\varphi}} \tag{20}$$

### 3.3 Stress distribution in the elastic zone

In the elastic zone, the stress of the surrounding rocks of the borehole followed the differential equation of stress balance (6) and showed the following relationship:

$$\sigma_r^p + \sigma_\theta^p = 2\sigma_0 \tag{21}$$

Substituting Eq. (21) into Eq. (6), we obtained the following:

$$\sigma_r^p = \sigma_0 - \frac{C_3}{r^2} \tag{22}$$

where $C_3$ is a constant.

The following boundary conditions exist in the elastic and plastic zones: when $r=R_s$, $\sigma_r{}^R=\sigma_r{}^s$, and $c_p=c_s$. Substituting this into Eqs. (17) and (20), we obtained the following:

$$\sigma_r^p|_{r=R_s} = \sigma_0(1-\sin\varphi) - c_p\cos\varphi \tag{23}$$

Using Eqs. (22) and (23), we obtained the following:

$$C_3 = R_s^2\left(\sigma_0\sin\varphi + c_p\cos\varphi\right) \tag{24}$$

The radial stress distribution equation in the elastic zone can be obtained as follows by substituting Eq. (24) into Eq. (22):

$$\sigma_r^p = \sigma_0 - \frac{R_s^2}{r^2}\left(\sigma_0\sin\varphi + c_p\cos\varphi\right) \tag{25}$$

The tangential stress distribution equation in the elastic zone can be obtained as follows by substituting Eq. (25) into Eq. (21):

$$\sigma_\theta^p = \sigma_0 + \frac{R_s^2}{r^2}\left(\sigma_0\sin\varphi + c_p\cos\varphi\right) \tag{26}$$

## 4 Variation law of stress and plastic zone of surrounding rocks of the borehole considering strain-softening

To explore the variation laws of stress and the plastic zone of surrounding rocks of the borehole considering strain-softening, we established the numerical model of the gas extraction borehole using the COMSOL numerical simulation software. The Mohr–Coulomb constitutive model is selected, and the theoretical Eq. (3) of the strain-softening model is introduced into the model (Deng et al. 2018), assuming that the surrounding rock of the borehole is in a two-way isobaric state. As the length of the gas extraction borehole is much larger than its diameter, the model can be simplified into a two-dimensional plane-strain model. The model is shown in Fig. 6; the model size is 10 × 10 m, and the parameters used in the numerical calculation are presented in Table 4.

## 4.1 Influence of residual cohesion on stress and plastic zone of borehole surrounding rock and model verification

### *4.1.1 Influence of residual cohesion on stress of borehole surrounding rock*

To study the influence of residual cohesion $c_r$ on the stress of surrounding rocks of the borehole, during numerical model calculations, the residual cohesion ($c_r$) values are set as 0.2, 0.3, 0.4, 0.5, 0.6, and 1.0 MPa, respectively (a residual cohesion of 1.0 MPa implies that the strain-softening of coal and rock is not considered), while the borehole radius is maintained at 0.2 m. The tangential stress distribution of

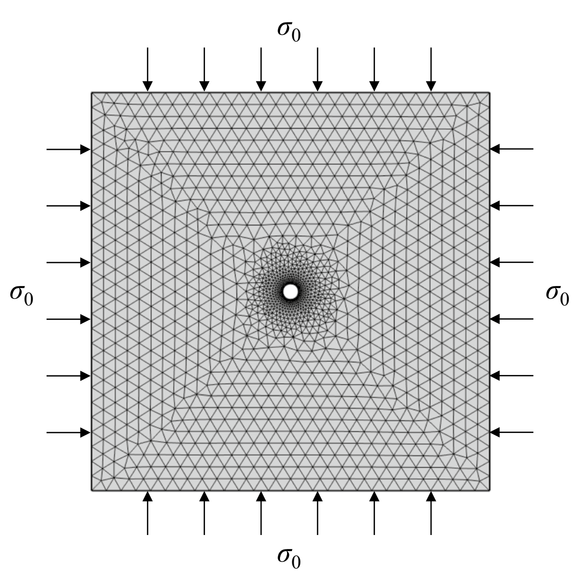


**Fig. 6** Model diagram

**Table 4** Parameters of the numerical simulation calculation

| Parameters | Value |
|---|---|
| Initial in-situ stress $\sigma_0$/MPa | 10.0 |
| Elastic modulus $E$/GPa | 1.0 |
| Internal friction angle $\varphi$/° | 30 |
| Poisson's ratio $\upsilon$ | 0.3 |
| Density $\rho$/kg/m$^3$ | 1400 |
| Peak cohesion $c_p$/MPa | 1.0 |

surrounding rocks of the borehole under different residual cohesions is shown in Fig. 7.

Figure 7 shows that the tangential stress of the surrounding rocks of boreholes initially increases and then decreases from the borehole boundary to the model boundary, gradually approaching the initial in-situ stress. With decreasing residual cohesion, the range of the stress increase zone increases gradually. The distance between the position of the stress peak and the borehole boundary also gradually increases, indicating that with decreasing residual cohesion, the stress of the surrounding rocks of the borehole is transferred to the deep; the lower the residual cohesion, the farther the distance to the deep part. Simultaneously, we also observed that the tangential stress at the borehole boundary gradually increases with increasing residual cohesion. Our analysis shows that the reduction of residual cohesion will reduce the bearing capacity of the surrounding rock at the shallow part of the borehole and reduce the force shared by this part, thus leading to the transfer of the peak stress to the deep part of the coal body. To observe the tangential stress distribution characteristics of the surrounding rocks of the borehole under different residual cohesion conditions, the tangential stress of the surrounding rocks of the borehole is expressed as a curve, as shown in Fig. 8.

Figure 8 shows that when the residual cohesion values are 0.2, 0.3, 0.4, 0.5, and 0.6 MPa, the depths of the peak stress transfer of surrounding rocks are 0.346, 0.229, 0.144, 0.099, and 0.056 m, respectively, compared with those when strain-softening is not considered. Simultaneously, under different residual cohesion conditions, the peak value of the tangential stress of the borehole surrounding rock changes slightly, which is about 16 MPa. The error is small when the peak stress is calculated by substituting the parameters into Eq. (25). When the residual cohesion

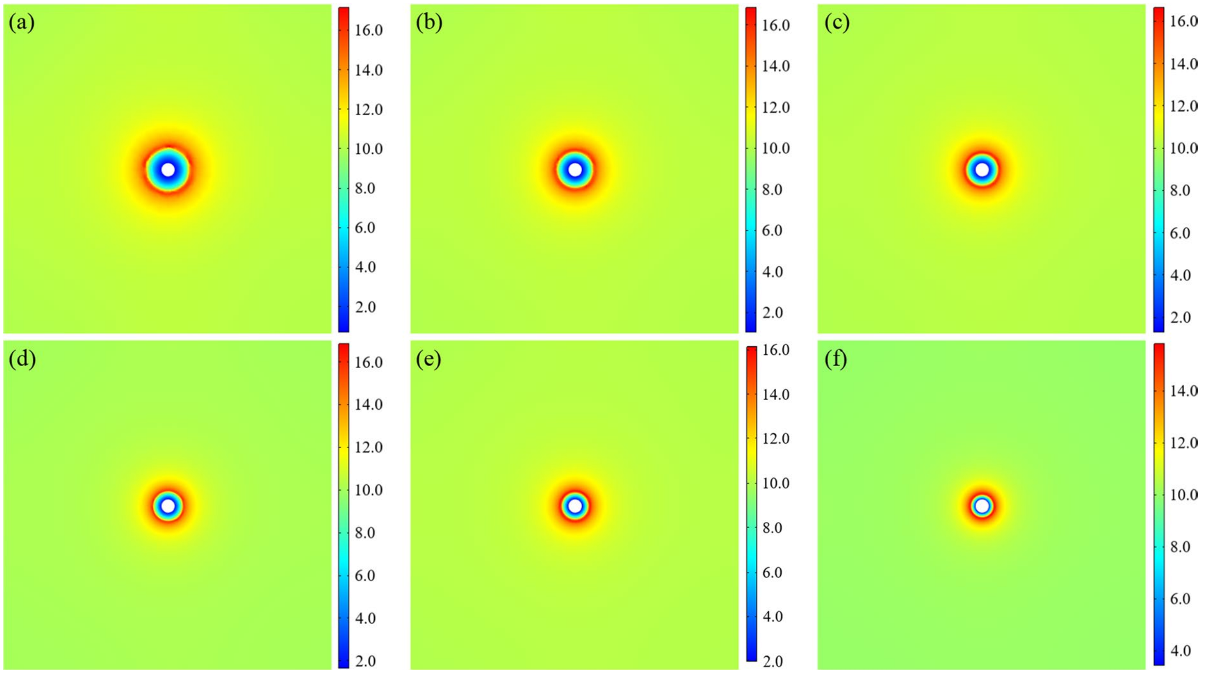


**Fig. 7** Tangential stress distribution of surrounding rocks of the borehole under different residual cohesions (MPa): **a** 0.2 MPa; **b** 0.3 MPa; **c** 0.4 MPa; **d** 0.5 MPa; **e** 0.6 MPa; and **f** 1.0 MPa

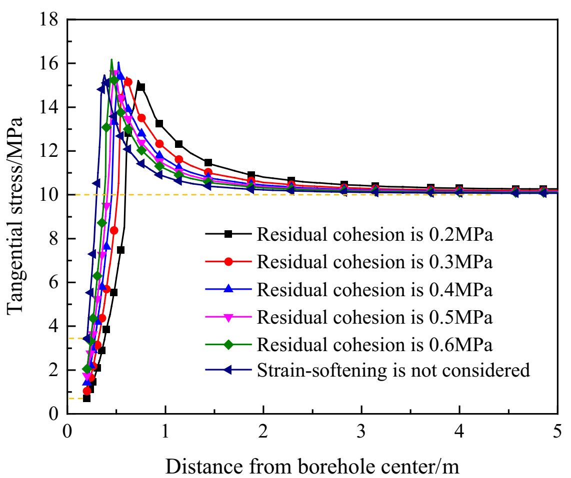


**Fig. 8** Tangential stress distribution curves of surrounding rocks of the borehole with different residual cohesion values

values are 0.2, 0.3, 0.4, 0.5, and 0.6 MPa when strain-softening is not considered, the tangential stress values of surrounding rocks at the borehole boundary are 0.694, 1.041, 1.423, 1.745, 2.049, and 3.428 MPa, respectively. At the borehole boundary, when $r=R_0$, the theoretical value of the tangential stress of surrounding rocks can be determined by Eq. (12). After substituting the parameters, the comparison between the results of theoretical calculation and numerical simulation is presented in Table 5. Notably, the maximum and minimum errors between the numerical simulation value of tangential stress at the borehole boundary and the theoretically calculated value are 2.670 and 0.144%, respectively. Moreover, the absolute error of the numerical simulation and theoretical calculation is less than 3.0%, indicating the accuracy of the numerical simulation results.

#### *4.1.2 Influence of the residual cohesion on the plastic zone of surrounding rocks of borehole*

To study the influence of residual cohesion $c_r$ on the plastic zone of surrounding rocks of the borehole, for numerical model calculations, the values of residual cohesion $c_r$ are set as 0.2, 0.3, 0.4, 0.5, 0.6, and 1.0 MPa, respectively (a residual cohesion of 1.0 MPa implies that the strain-softening of coal and rock is not considered). Meanwhile, the borehole radius remains unchanged at 0.2 m, and the plastic zone is

**Table 5** Comparison between the theoretically calculated and numerical simulation values of tangential stress at the borehole boundary

| Residual cohesion $c_r$/MPa | Theoretical calculation value /MPa | Numerical simulation value /MPa | Error /% |
|---|---|---|---|
| 0.2 | 0.693 | 0.694 | 0.144 |
| 0.3 | 1.039 | 1.041 | 0.192 |
| 0.4 | 1.386 | 1.423 | 2.670 |
| 0.5 | 1.732 | 1.745 | 0.751 |
| 0.6 | 2.078 | 2.049 | − 1.396 |
| 1.0 (Strain-softening is not considered) | 3.464 | 3.428 | − 1.039 |

bounded by an equivalent plastic shear strain equal to 0. The range of the plastic zone of surrounding rocks of the borehole under different cohesion conditions is shown in Fig. 9.

Figure 9 shows that under the two-way isobaric state, the plastic zone of surrounding rocks of the borehole is distributed in a circular shape. With increasing residual cohesion, the range of the plastic zone of surrounding rocks of the borehole gradually decreases. The numerical simulation results show that when the residual cohesion values are 0.2, 0.3, 0.4, 0.5, and 0.6 MPa and strain-softening is not considered, the plastic zone radii of surrounding rocks of the borehole are 0.723, 0.606, 0.521, 0.476, 0.433, and 0.377 m, respectively. The theoretical value of the plastic zone radius of surrounding rocks of the borehole considering strain-softening can be determined by Eq. (20), and that without considering strain-softening can be determined by Eq. (27) (Qian et al. 2010). After substituting the parameters, the

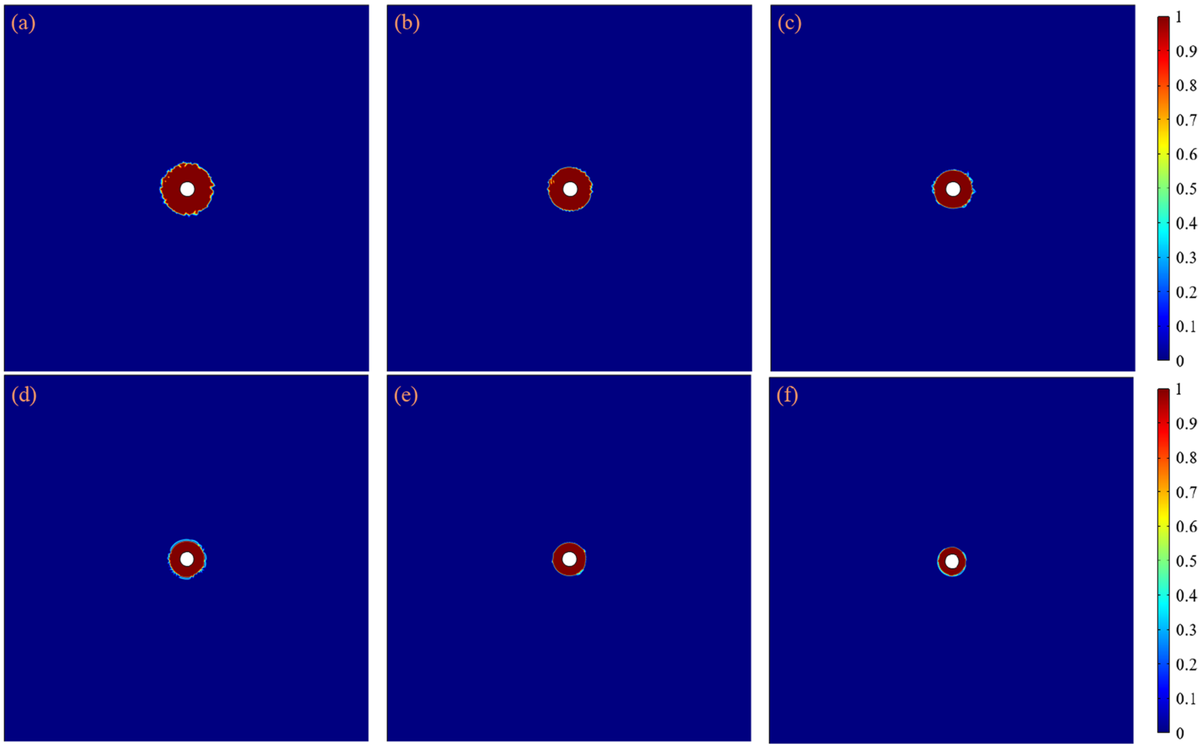


**Fig. 9** Plastic zone range of surrounding rocks of the borehole under different residual cohesion conditions: **a** 0.2 MPa; **b** 0.3 MPa; **c** 0.4 MPa; **d** 0.5 MPa; **e** 0.6 MPa; and **f** 1.0 MPa

theoretical calculation results and numerical simulation results are presented in Table 6. Notably, the maximum and minimum errors between the numerical simulation and theoretically calculated values of surrounding rocks of the borehole are 8.924 and 2.446%, respectively. The absolute error value of the numerical simulation and theoretical calculation is less than 10.0%, indicating the accuracy of the numerical simulation of the plastic zone radius of surrounding rocks of the borehole.

$$R_s = R_0 \left[ \frac{\left(\sigma_0 + c_p \cot \varphi\right)(1 - \sin \varphi)}{c_p \cot \varphi} \right]^{\frac{1-\sin \varphi}{2 \sin \varphi}} \tag{27}$$

In summary, the peak value of the tangential stress of the surrounding rocks of the borehole, the tangential stress value of the borehole boundary, and the plastic zone radius of the surrounding rocks of the borehole calculated by numerical simulation have slight errors compared with those from the theoretical calculation results, indicating the accuracy of the established model.

## 4.2 Variation law of stress and plastic zone in surrounding rocks of boreholes of different radii considering strain-softening

Hydraulic flushing gas extraction technology uses a high-pressure water jet to break the coal body and flush the coal body out under the action of water flow. This expands the radius of the ordinary borehole by several fold or even more than ten-fold and can improve the gas extraction effect. Hydraulic flushing technology can change the radius of the borehole by controlling the coal flushing amount according to specific requirements. Therefore, it is necessary to study the variation law of the stress and plastic zone of surrounding rocks of the borehole with different radii considering strain-softening. The COMSOL numerical simulation software is used to establish the same numerical calculation model shown in Fig. 5. The residual cohesion $c_r$ is set to 0.5 MPa. Except for the borehole radius, other parameters are the same, as presented in Table 4. We studied the variation law of stress and plastic zone of surrounding rocks of the borehole with borehole radii of 0.1, 0.2, 0.3, and 0.4 m, respectively.

### 4.2.1 *Variation law of stress of surrounding rocks of boreholes with different radii*

The simulation results of the tangential stress distribution of surrounding rocks of boreholes with different radii, both without considering strain-softening and considering strain-softening, are shown in Figs. 10 and 11.

Figures 10 and 11 show that regardless of whether strain-softening is considered or not, with increasing borehole radius, the tangential stress of surrounding rocks of the borehole increases with increasing distance away from the borehole center. This indicates that the increase in borehole radius will increase the stress reduction zone of the surrounding rocks of the borehole and transfer the high stress of the surrounding rocks of the borehole to the deep part. Under the same borehole radius, the distance from the borehole center to the tangential stress peak of surrounding rocks of the borehole considering strain-softening increased compared with that without considering strain-softening. Our analysis shows that the larger the borehole radius, the stronger the disturbance to the surrounding rock of the borehole, and the lower part of the bearing

**Table 6** Comparison between the theoretically calculated and numerical simulation values of the plastic zone radius of surrounding rocks of the borehole

| Residual cohesion $c_r$/MPa | Theoretical calculation value/m | Numerical simulation value/m | Error/% |
|---|---|---|---|
| 0.2 | 0.691 | 0.723 | 4.631 |
| 0.3 | 0.564 | 0.606 | 7.447 |
| 0.4 | 0.489 | 0.521 | 6.544 |
| 0.5 | 0.437 | 0.476 | 8.924 |
| 0.6 | 0.399 | 0.433 | 8.521 |
| 1.0 (Strain-softening is not considered) | 0.368 | 0.377 | 2.446 |

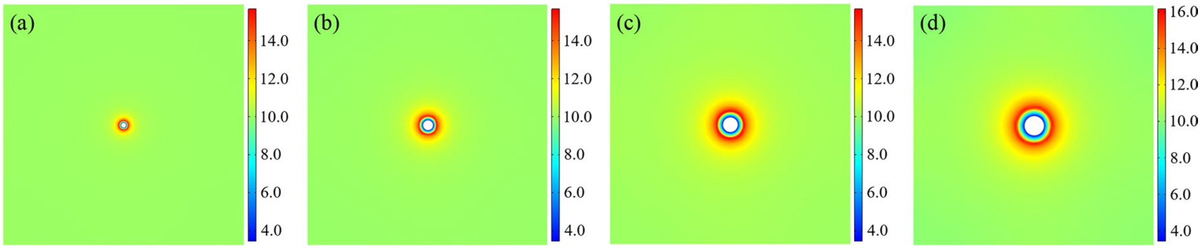


**Fig. 10** Cloud chart of the tangential stress distribution in surrounding rocks of boreholes with different radii without considering strain-softening: **a** 0.1 m; **b** 0.2 m; **c** 0.3 m; and **d** 0.4 m

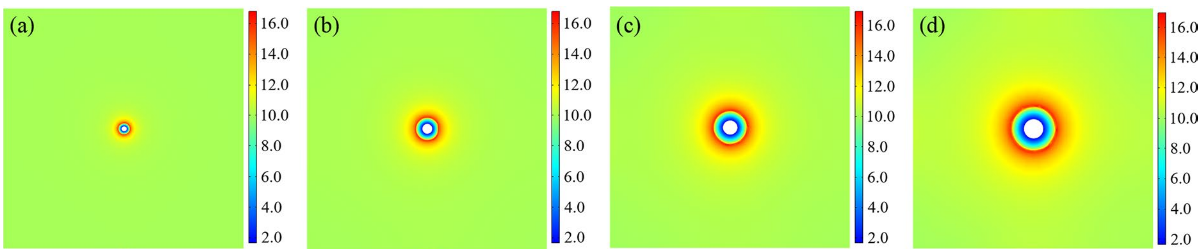


**Fig. 11** Cloud chart of the tangential stress distribution in surrounding rocks of boreholes with different radii considering strain-softening: **a** 0.1 m; **b** 0.2 m; **c** 0.3 m; and **d** 0.4 m

capacity of the surrounding rock of the borehole increases. Therefore, there can be a transfer of the peak stress to the depth. The tangential stress distribution curve of surrounding rock under the same borehole conditions is shown in Fig. 12.

Figure 12 shows that when the borehole radii were 0.1, 0.2, 0.3, and 0.4 m, the distances between the tangential stress peak considering strain-softening and the borehole center increased by 0.045, 0.099, 0.123, and 0.172 m, respectively, compared with those without considering strain-softening. When strain-softening is not considered, with borehole radii of 0.2, 0.3, and 0.4 m, the distances of the peak value of tangential stress transfer to the deep part of surrounding rocks were 0.185, 0.383, and 0.589 m, respectively, as opposed to those for a borehole radius of 0.1 m. When considering strain-softening, with borehole radii of 0.2, 0.3, and 0.4 m, the distances of the peak value of tangential stress transfer to the deep part of surrounding rocks were 0.239, 0.461, and 0.716 m, respectively, as opposed to those with a borehole radius of 0.1 m. Simultaneously, we observed that the tangential stress at the borehole boundary remains unchanged with increasing borehole radius, regardless of whether strain softening was considered.

#### 4.2.2 *Variation law of the plastic zone of surrounding rocks of boreholes with different radii*

The distribution ranges of the plastic zone of surrounding rocks of the borehole with different radii without and with considering strain-softening are shown in Figs. 13 and 14.

Figures 13 and 14 show that, regardless of whether strain-softening was considered or not, with increasing borehole radius, the plastic zone radius of surrounding rocks of the borehole gradually increases. When strain-softening is not considered, the plastic zone radii are 0.192, 0.377, 0.575, and 0.781 m while the borehole radii are 0.1, 0.2, 0.3, and 0.4 m, respectively. When considering strain-softening, the plastic zone radii are 0.237, 0.437, 0.698, and 0.953 m while the borehole radii are 0.1, 0.2, 0.3, and 0.4 m, respectively. We found that under the same borehole radius, the plastic zone radius when considering strain-softening is more significant than when strain-softening is not considered. To observe the influence of the borehole radius on the plastic zone of surrounding rocks when considering strain-softening, the variation of the plastic zone radius with borehole radius with

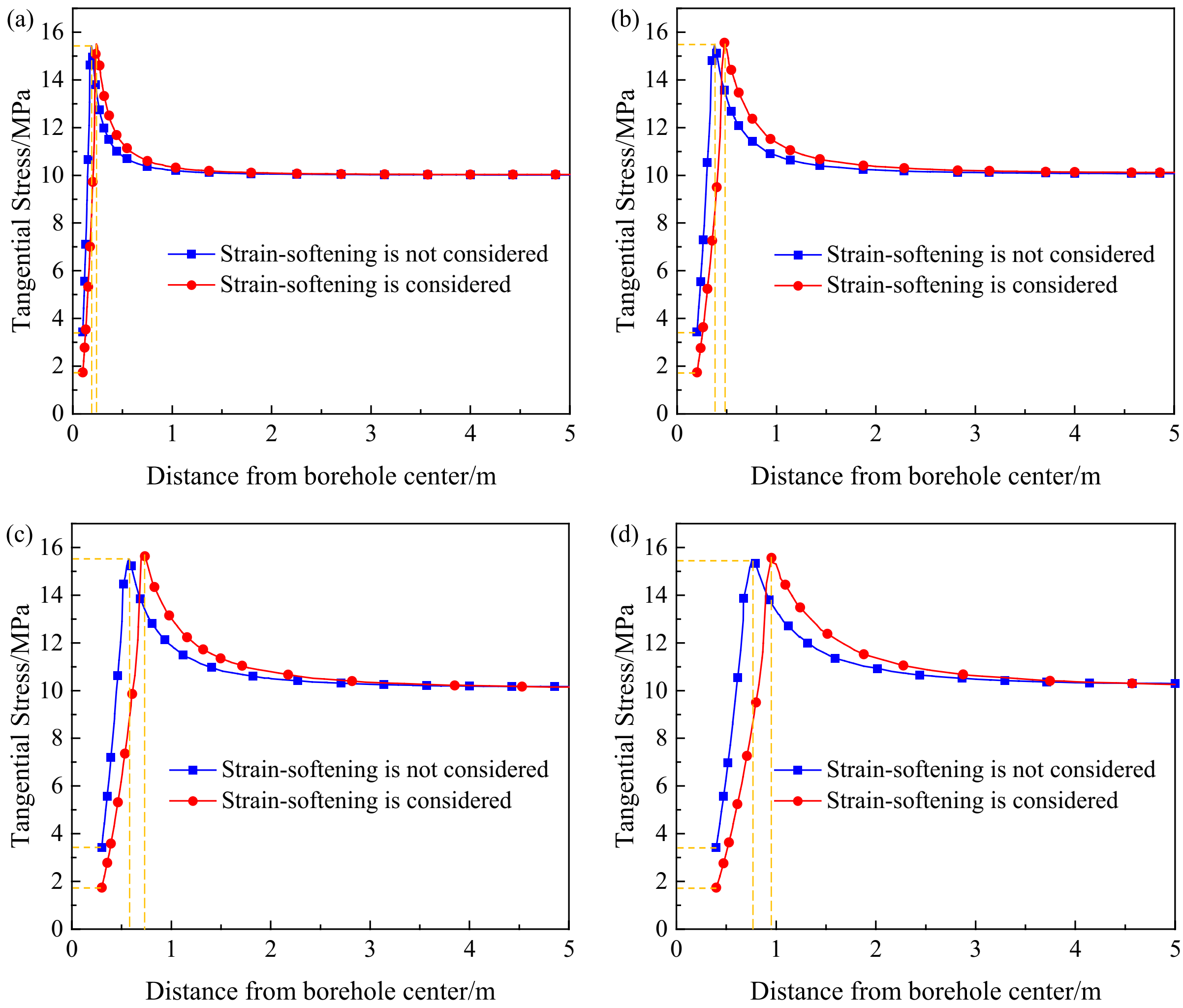


**Fig. 12** Tangential stress distribution curve of surrounding rocks of boreholes with different radii without considering strain-softening and considering strain-softening: **a** 0.1 m; **b** 0.2 m; **c** 0.3 m; and **d** 0.4 m

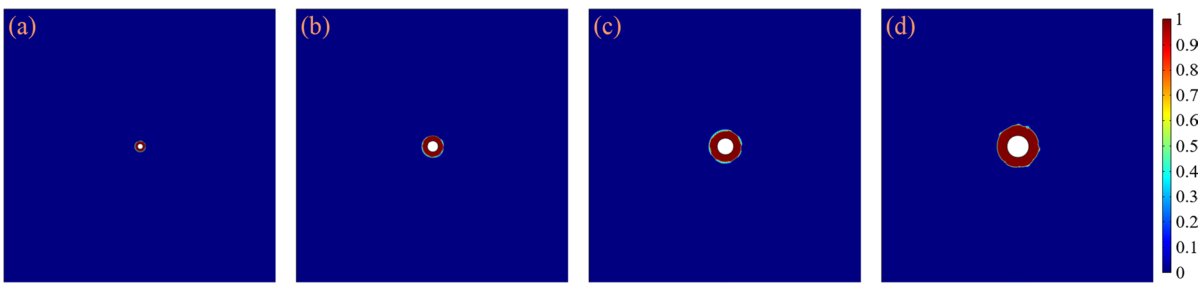


**Fig. 13** The distribution ranges of the plastic zone of surrounding rock of boreholes with different radii without considering strain-softening: **a** 0.1 m; **b** 0.2 m; **c** 0.3 m; and **d** 0.4 m

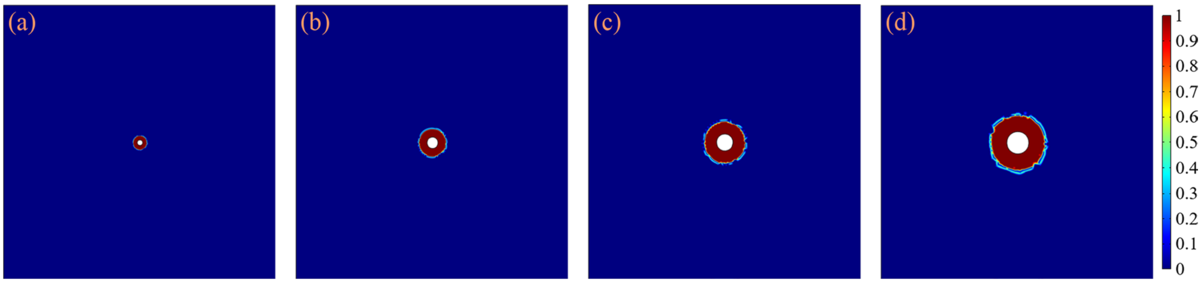


**Fig. 14** The distribution ranges of the plastic zone of surrounding rocks of boreholes with different radii considering strain-softening: **a** 0.1 m; **b** 0.2 m; **c** 0.3 m; and **d** 0.4 m

and without considering strain-softening is expressed as a curve, as shown in Fig. 15. This figure shows that a linear relationship exists between the plastic zone radius and borehole radius. The larger the borehole radius, the greater the impact of strain-softening on the plastic zone.

Based on the study of the tangential stress and plastic zone of surrounding rocks of boreholes with different radii, we found that in gas extraction boreholes, it is necessary to consider the strain-softening of surrounding rocks. This is especially true for a hydraulic flushing borehole, wherein the borehole radius can usually reach more than 0.4 m; thus, the strain-softening of surrounding rocks should be considered.

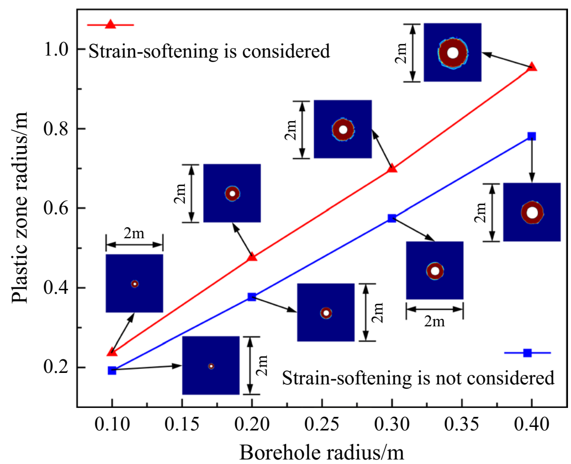


**Fig. 15** Comparison of variation curves of the plastic zone radius with borehole radius with and without considering strain-softening

## 5 Field verification of strain-softening of surrounding rocks of the borehole

To investigate the temporal and spatial evolution law of in-situ coal stress around the hydraulic flushing borehole, Wang et al. (2020) considered the No. 21 outburst coal seam of Liangbei coal mine, Henan Province, as the engineering background. They conducted the synchronous monitoring of the regional in-situ stress field of the cross-measure hydraulic flushing borehole by using the self-developed stress monitoring system. The equipment and test location used in the paper are shown in Fig. 16. They concluded that the stress reduction zone is within 4 m from the hydraulic flushing borehole center, the stress transition zone is between 4 and 5 m, the stress concentration zone is beyond 5 m, and the radius of the stress reduction zone is about 10 times the equivalent radius of the hydraulic flushing borehole. The stress distribution of surrounding rocks of the hydraulic flushing borehole measured on site is shown in Fig. 17. Combined with the published papers of Han (2020), the parameters of the No. 21 coal seam in Liangbei coal mine, Henan Province can be determined, as presented in Table 7. According to the research in the second part of this paper, the residual cohesion of coal and rock can be reduced by more than 99% compared to peak cohesion. We assumed that the residual cohesion of the No. 21 coal seam in Liangbei coal mine, Henan Province reduced by 95% compared with the peak cohesion; namely, the residual cohesion is 0.075 MPa.

We established the numerical calculation model (the same as Fig. 5) according to the coal seam, borehole parameters, and residual cohesion $c_r$. The model size was increased to 20×20 m to reduce the

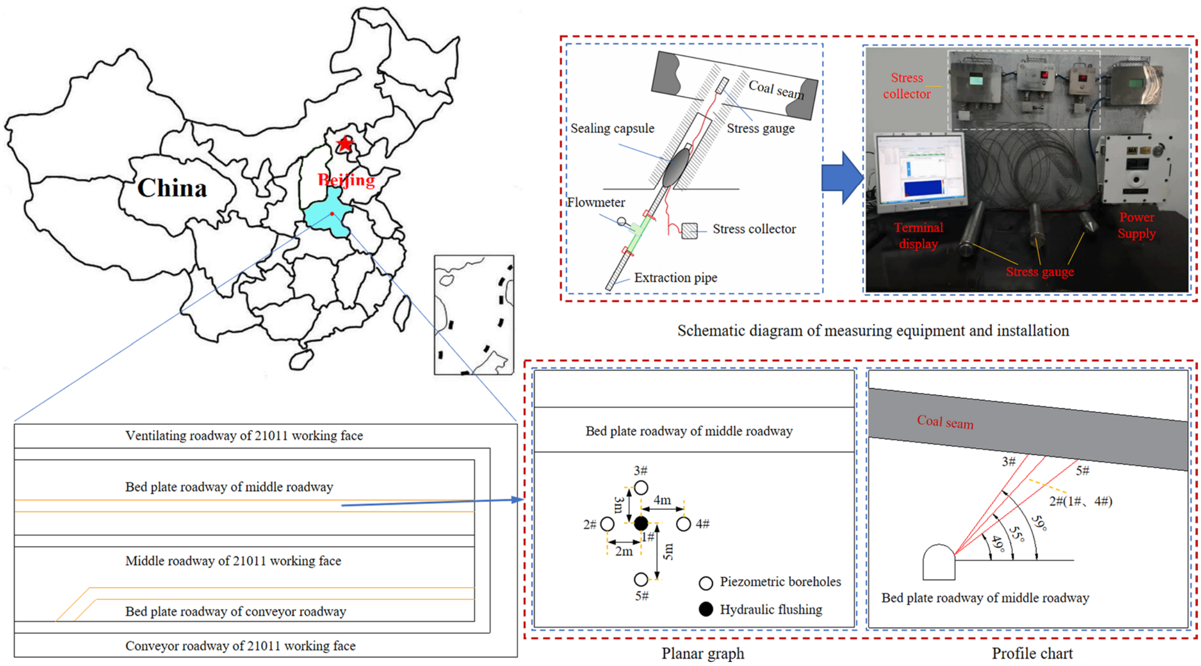


**Fig. 16** The equipment and test location (Wang et al. 2020)

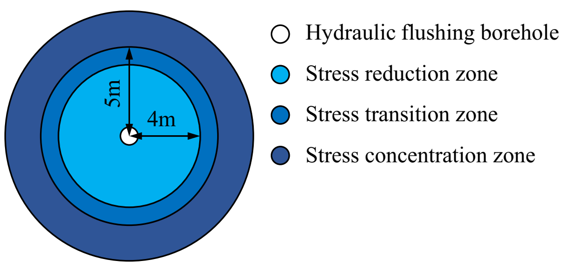


**Fig. 17** Field measured stress distribution of surrounding rocks of the hydraulic flushing borehole (Wang et al. 2020)

**Table 7** Parameters of the No. 21 coal seam in the Liangbei coal mine, Henan Province

| Parameters | Value |
|---|---|
| Initial in-situ stress of coal seam $\sigma_0$/MPa | 7.0 |
| Elastic modulus of coal seam $E$/GPa | 1.2 |
| Internal friction angle of coal seam $\varphi$/° | 20 |
| Poisson's ratio of coal seam $\upsilon$ | 0.46 |
| Density of coal seam $\rho$/kg/m$^3$ | 1440 |
| Peak cohesion of coal seam $c_p$/MPa | 1.5 |
| Borehole radius $R_0$/m | 0.4 |

influence of the boundary. The comparison of the simulation results of the tangential stress distribution curve, plastic zone radius, and stress reduction zone radius of surrounding rocks of the borehole without and with considering strain-softening is shown in Figs. 18, 19 and 20.

Figures 18, 19 and 20 show that the peak stress depth, plastic zone radius, and stress reduction zone radius of surrounding rocks of the borehole when strain-softening is considered are far greater than those when strain-softening is not considered. When strain-softening was not considered, the plastic zone and stress reduction zone radii were 0.707 m (theoretical value was 0.695 m) and 0.522 m, respectively. When strain-softening was considered, the plastic zone and stress reduction zone radii were 3.416 m (theoretical value was 3.379 m) and 2.665 m, respectively. When strain-softening was not considered, the calculated stress reduction zone radius was 1.305 times the borehole radius; when strain-softening was considered, the calculated stress reduction zone radius was 6.663 times the borehole radius. Comparing the results measured on the field with those from the simulation, we found that the simulation results were smaller than those in the

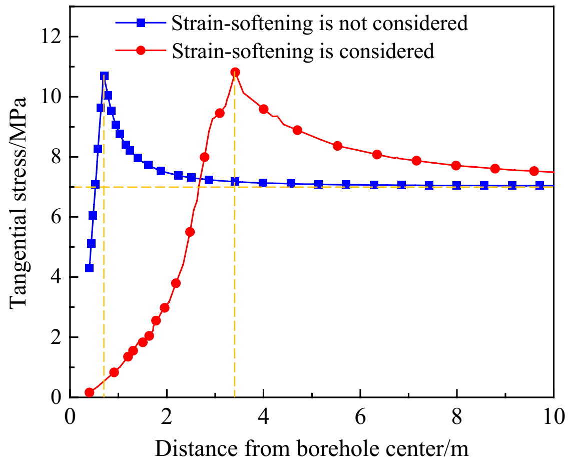


**Fig. 18** Tangential stress distribution curve of surrounding rocks of the borehole

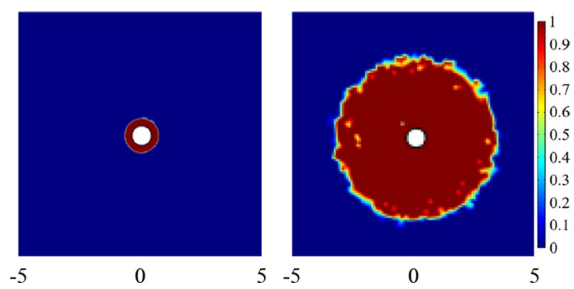


**Fig. 19** Distribution ranges of the plastic zone of surrounding rocks of the borehole when: **a** strain-softening is not considered; and **b** strain-softening is considered

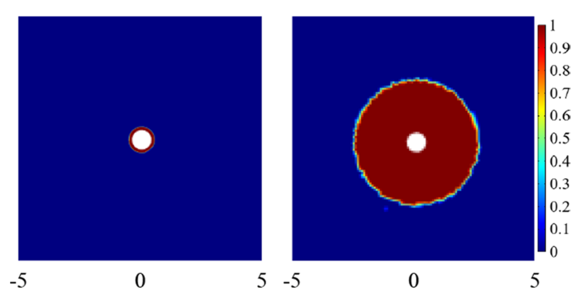


**Fig. 20** Distribution ranges of the stress reduction zone of surrounding rocks of the borehole when: **a** strain-softening is not considered; and **b** strain-softening is considered

field, regardless of whether strain-softening was considered. However, compared with the result without considering strain-softening, that considering strain-softening was closer to the result measured in the field. This indicated that strain-softening does occur in the field, which is an essential factor for the significant difference between the field-measured stress distribution results and previous theoretical calculation results.

## 6 Conclusion

1. Through the analysis of previous experimental data, we proved that the essence of strain-softening of coal and rock is that the internal friction angle remains unchanged, and the cohesion decreases. According to the variation law of cohesion, we theoretically analyzed the stress distribution of the crushing, plastic, and elastic zones of the borehole surrounding rock when considering strain-softening. We also provided the theoretical equation for the plastic zone radius of the surrounding rocks of the borehole.
2. We established a two-dimensional plane-strain model for a borehole by considering strain-softening. The influence of residual cohesion on the stress and plastic zone of surrounding rocks of the borehole is simulated and analyzed. We found that with decreasing residual cohesion, the peak stress of surrounding rocks of the borehole will be transferred to the deep part, and the radius of the plastic zone will gradually increase. The simulated peak tangential stress value, the tangential stress value of the borehole boundary, and the plastic zone radius are compared with those calculated theoretically. We found that the error is less than 10%, which verifies the model's accuracy.
3. We studied the influence law of strain-softening on the stress and plastic zone of surrounding rocks of boreholes with different radii. We found that the larger the borehole radius, the greater the difference between the peak stress of surrounding rocks and the borehole center when considering strain softening, and the greater the difference in the radius of the plastic zone.
4. The field measurement results show that the stress reduction zone radius of the hydraulic flushing borehole is about 10 times the borehole radius. When strain-softening is not considered, the stress reduction zone radius calculated by the

simulation is 1.305 times the borehole radius; when strain-softening is considered, the stress reduction zone radius obtained by the simulation is 6.663 times the borehole radius. Considering that the calculated result of the strain-softening model is closer to reality, we proved that strain-softening is an important factor influencing the large difference between the measured stress distribution results and the previous theoretical calculation results.

**Acknowledgements** This work was financially supported by the National Natural Science Foundation of China (Grant No. 52074296, 52004286), the China Postdoctoral Science Foundation (Grant No. 2020T130701, 2019M650895), the State Key R&D Plan (2017YFC0804303) of the Ministry of Science and Technology of China.

**Declarations**

**Competing interest** The authors declare that they have no known competing financial interests or personal relationships that could have appeared to influence the work reported in this paper.



## References

Alonso E, Alejano LR, Varas F, Fdez-Manin G, Carranza-Torres C (2003) Ground response curves for rock masses exhibiting strain-softening behaviour. Int J Numer Anal Methods Geomech 27:1153–1185

Cao RH, Cao P, Zhang K, Lin H (2013) Stability analysis of roadway intersection considering strain softening. Rock Soil Mech 34:73–77

Cao ZY, He XQ, Wang EY, Pan C, Zhao X, Ji PJ (2018) Law of methane emission and its controlling factors in the blind reverse fault zone. J Min Saf Eng 35:657–662

Cao ZY, Wang EY, He XQ, Wang H, Liu QL, Zhang GH, Luo F, Wang C, Xu YL (2021) Effect evaluation of pressure relief and gas drainage of hydraulic punching in short-distance coal seam group with the risk of outburst. J Min Saf Eng 38:634–642

Chen DD, He WR, Xie SR, He FL, Zhang Q, Qin BB (2020) Increased permeability and coal and gas outburst prevention using hydraulic flushing technology with cross-seam borehole. J Nat Gas Sci Eng 73:1–16

Deng Q, Tang H, Wang DY, Qin YQ, Wu ZJ (2018) Bench-shape slope stability analysis based on strain softening model. Rock Soil Mech 39:4109–4116

Gao YB, Lin BQ, Yang W, Li ZW, Pang Y, Li H (2015) Drilling large diameter cross-measure boreholes to improve gas drainage in highly gassy soft coal seams. J Nat Gas Sci Eng 26:193–204

Gao Y, Liang P, Zhou Y (2020) Strength criterion effect on elasto-plastic solution of deep tunnels considering strain softening characteristics. J Cent South Univ (sci Technol) 51:2525–2537

Ge Z, Mei X, Jia Y, Lu Y, Xia W (2014) Influence radius of slotted borehole drainage by high pressure water jet. J Min Saf Eng 3:657–664

Han X (2020) Research and application of the influence law of the angle between borehole and coal seam on hydraulic flushing effect. China University of Mining and Technology 24–25

Hao FC, Sun LJ, Liu MJ (2014) Research on boreholes space optimization of hydraulic flushing considering press relief and gas drainage effect. J Min Saf Eng 31:756–763

He C, Tang H, Shen P, Su X (2021) Progressive failure mode and stability reliability of strain-softening slope. Eart Sci 46:697–707

Jaiswal A, Shrivastva BK (2009) Numerical simulation of coal pillar strength. Int J Rock Mech Min Sci 46:779e788

Jing W, Xue WP, Yao ZS (2018) Variation of the internal friction angle and cohesion of the plastic softening zone rock in roadway surrounding rock. J China Coal Soc 43:2203–2210

Joshua P, Thomas S, Vikas T (2019) Plastic strain gradients and transient fatigue crack growth: a computational study. Int J Fatigue 120:283–293

Kong LA, Hao FC, Liu MJ, Xin XP, Wei GY (2005) Hydraulic flushing rapid tunneling technology. Saf Coal Mines 36:46–48

Kong XG, Wang EY, Liu XF, Li N, Chen L, Feng JJ, Kong B, Li DX, Liu QL (2016) Coupled analysis about multi-factors to the effective influence radius of hydraulic flushing: Application of response surface methodology. J Nat Gas Sci Eng 32:538–548

Leandro A, Alfonso RD, Maria V (2012) Plastic radii and longitudinal deformation profiles of tunnels excavated in strain-softening rock masses. Tunn Undergr Sp Technol 30:169–192

Li P, Wang K, Jiang YF, Gou JQ (2015) Applied study on hydraulic reaming technology of mining seam in Hongling Mine. Coal Sci Technol 43:69–73

Liang P, Gao Y, Zhou Y, Deng D (2022) Determination method and engineering application of reasonable installation timing of the initial ground support. Chin J Eng 44:265–276

Lin BQ, Zhang JG (1996) Theory and technology of mine gas drainage. China University of Mining and Technology Press, Xuzhou, pp 66–123
Liu MJ, Kong LA, Hao FC, Xin XP, Wei GY, Liu YW (2005) Application of hydraulic flushing technology in severe outburst coal. J China Coal Soc 30:451–454
Liu YW, Ren PL, Xia SB, Sun YG (2009) Analysis of pressure-relief and permeability improvement effect of hydraulic flushing. J Henan Polytech Univ (nat Sci) 28:695–699
Pan JL, Gao ZN, Ren FH (2018) Effect of strength criteria on surrounding rock of circular roadway considering strain softening and dilatancy. J China Coal Soc 43:3293–3301
Qian MG, Shi PW, Xu JL (2010) Ground pressure and strata control. China University of Mining and Technology Press, Beijing, pp 59–60
Shen RX, Qiu LM, Lv GG, Wang EY, Li HR, Han X, Zhang X, Hou ZH (2018) An effect evaluation method of coal seam hydraulic flushing by EMR. J Nat Gas Sci Eng 54:154–162
Su CD, Fu YS (2014) Experimental study of triaxial compression deformation and strength characteristics of red sandstone. Chin J Rock Mech Eng 33:3164–3169
Tao YQ, Zhang CL, Xu J, Peng SJ, Feng D (2018) Effect evaluation on pressure relief and permeability improvement of hydraulic flushing physical experiment. J Chongqing Univ 41:69–77
Wang EY, Wang H, Liu XF, Shen RX, Zhang CL (2020) Spatio temporal evolution of geostress and gas field around hydraulic punching borehole in coal seam. Coal Sci Technol 48:39–45
Wang FY, Qian DL (2018) Elasto-analysis for a deep tunnel considering intermediate stress and strain-softening behavior. J China Coal Soc 43:3329–3337
Wang XX, Xia SB, Shi BM, Mu CM (2011) Experiment research on hydraulic borehole flushing in No.13-1 seam of Pansan Mine. Coal Sci Technol 39:60–64
Wang XX, Shi BM, Mu CM (2012) Study on formation mechanism of gas emission partition in hydraulic flushing coal seam. J China Coal Soc 37:467–471
Wang K, Li B, Wei JP, Li P (2013) Change regulation of coal seam permeability around hydraulic flushing borehole. J Min Saf Eng 30:778–784
Wang ZF, Sun XM, Lu TK, Han YB (2015) Experiment research on strengthening gasdrainage effect with fracturing technique by liquid CO 2 phase transition. J Henan Polytech Univ (nat Sci) 34(1):1–5
Wang M, Song ZF, Zheng DJ, Shen WL, Gou PF, Wei SJ (2021) Development and application of rock energy dissipation model in FLAC3D. J China Coal Soc 46:2565–2573
Wei J, Li B, Wang K, Sun D (2016) 3D numerical simulation of boreholes for gas drainage based on the pore–fracture dual media. Int J Min Sci Tech 26:739–744
Zhang TG (2001) Comprehensive treatment technology of mine gas. Coal Industry Press, Beijing, pp 265–267
Zhang J, Wang XD (2017) Permeability-increasing effects of hydraulic flushing based on flow-solid coupling. Geome Eng 13:285–300
Zhang CH, Zhao QS (2014) Triaxial tests of effects of varied saturations on strength and modulus for sandstone. Rock Soil Mech 35:951–958
Zhang H, Cheng YP, Yuan L, Wang L, Pan ZJ (2019) Hydraulic flushing in soft coal sublayer: gas extraction enhancement mechanism and field application. Energy Sci Eng 7:1970–1993
Zhang H, Cheng YP, Deng CB, Shu LY, Pan ZJ, Yuan L, Wang L, Liu QQ (2022) A novel in-seam borehole discontinuous hydraulic flushing technology in the driving face of soft coal seams: enhanced gas extraction mechanism and field application. Rock Mech Rock Eng 55:885–907
Zhou JW, Xu WY, Li MW, Zhou XQ, Shi C (2009) Application of rock strain softening model to numerical analysis of deep tunnel. Chin J Rock Mech Eng 28:1116–1127
Zuo JP, Chen Y, Zhang JW, Wang JT, Sun YJ, Jiang GH (2016) Failure behavior and strength characteristics of coal-rock combined body under different confining pressures. J China Coal Soc 41:2706–2713